Int. J. Electrochem. Sci., 13 **(2018)** 8198 – 8221, doi: 10.20964/2018.08.79

International Journal of ELECTROCHEMICAL SCIENCE
www.electrochemsci.org

Effect of *Mentha Piperita* essential oil on mild steel corrosion in hydrochloric acid

Z. Bensouda[1], M. Driouch[1], M. Sfaira[1], A. Farah[2], M. Ebn Touhami[3], B. Hammouti[4], K.M. Emran[5,]*

[1] Laboratoire d'Ingénierie des Matériaux, de Modélisation et d'Environnement. Université Sidi Mohamed Ben Abdellah USMBA, Faculté des Sciences BP 1796-30000 Fès-Atlas, Morocco.
[2] Laboratoire de Chimie Organique Appliquée. Université Sidi Mohamed Ben Abdellah USMBA, Faculté des Sciences et Techniques. Route Immouzer Fès, Morocco.
[3] Laboratoire d'Ingénierie des Matériaux et Environnement : Modélisation et Application, Faculté des Sciences, Université Ibn Tofaïl, BP. 133-14000, Kénitra, Morocco.
[4] Laboratory of Applied Chemistry & Environment, Faculty of Science, Mohammed Premier University - B.P. 4808, 60046 Oujda - Morocco.
[5] Department of Chemistry, College of Science, Taibah University, Al-Madinah Al-Monawarah, PO Box4050, Saudi Arabia
[*]E-mail: kabdalsamad@taibahu.edu.sa; bensouda@yahoo.com

Received: 29 April 2018 / *Accepted:* 19 June 2018 / *Published:* 5 July 2018

The *Mentha Piperita* essential oil (MPEO) rich in anthraquinone,1-(p-fluorophen) as major compound (42.8 %) has been investigated as corrosion inhibitor for mild steel in 1 M HCl. weight loss, polarization curves (Tafel, Stern & Geary as well as Stern methods) and electrochemical impedance spectroscopy measurements were used to evaluate the inhibition performance of MPEO. The results obtained from different techniques were in best accord. The inhibiting efficiency, reaching circa 87 % at 0.7 g L^{-1} of MPEO, was found to increase with rise of inhibitor concentration, whereas the increase of temperature was in favour of its slow decrease. The adsorption data fitted well to Langmuir isotherm model and involved both physisorption. Scanning electron microscopic results testified the formation of a protective film onto the mild steel in the presence of MPEO.

Keywords: *Mentha Piperita*; Anthraquinone; Acid Corrosion; Inhibition; Adsorption isotherms.

1. INTRODUCTION

Corrosion is a natural phenomenon widely defined as degradation of metal surfaces in contact with an aggressive environment. The direct and indirect consequences of corrosion are quite many and are considered as a major problematic in industry, constructions and civil services. Mild steel appears to

be extensively used for structural applications because of its low cost. However, its susceptibility to be rusting in humid air and high dissolution rate in acidic solutions, are the major inconvenient for its use on larger scale without protection.

Hydrochloric acid is generally used in industries for cleaning, descaling and pickling of steel structures, such as reactors, agitators, pumps, drain, etc., which are subject of considerable metal dissolution. To slow down the aggressiveness of this acid, the use of inhibitors is the most practical protection method against corrosion process. Considerable synthetic compounds have been tested and are still being to evaluate their corrosion inhibition potential [1–5].

Though many synthetic molecules presented good potential against corrosion, the greater part of them is extremely toxicant to both human and environment. The safety and environmental issues of corrosion inhibitors, arisen in industries, have always been a global concern. The toxicity may manifest either during the synthesis of the molecules or during its application [6,7]. Consequently, as a result of environmental concern, for these synthetic compounds, researches into the practice of eco-friendly compounds, as green corrosion inhibitors, for mild steel have intensified to substitute toxic chemicals currently in use. Indeed, in the most recent decade, several studies have been completed on corrosion inhibition by using plant extract [8,9], purified compounds [10,11] and essential oils [12–21]. All of them have been announced as good inhibitors for different metals and alloys in different acidic media.

This study aims at the investigation of the effect of *Mentha Piperita* essential oil, denoted hereafter MPEO, on mild steel corrosion inhibition in molar hydrochloric solution. The extraction of MPEO is done by hydrodistillation using a Clevenger-type apparatus and identification of MPEO components is given by spectral analysis of gas chromatography coupled to mass spectrometry (GC–MS). The corrosion performance is conducted by coupling weight loss, electrochemical associated with scanning electron microscopy techniques. The adsorption and inhibition efficiency of MPEO inhibitor are investigated and the thermodynamic along with kinetic parameters in the absence and presence of MPEO are calculated and discussed.

2. EXPERIMENTAL

2.1 Plant material

Samples of *Mentha x Piperita L.* came from a land in the region of Kelâat Gouna (located in southern of Morocco, in the Souss-Massa-Draa and the province of Tinghir). The sample collection was done in the summer, during the flowering period of the plant. Only the aerial parts (leaves, flowers, stems) were collected.

2.2 Preparation

The extraction of *Mentha Piperita* was conducted by hydrodistillation in a Clevenger-type apparatus in the Laboratory of Green extraction of the Ex-National Institute of Medicinal and Aromatic Plants-Taounate in Morocco. The distillation was carried out by boiling for 2 h. The essential oil yield

was expressed in mL/100 g of dry matter. For the treated samples, the average yield of essential oil obtained was of 1.15 %.

The oil was dried over anhydrous Na_2SO_4. The MPEO was subjected to GC-MS (type QP2010Shimadzou) analysis using Trace GC/Polaris Q (GC-MS, ThermoElectron). The column was a VB-5 (5 % phenyl and 95 % dimethylpolysiloxan) with film thickness of 0.25 μm, a length of 30 m, and an internal diameter of 0.25 μm used with helium gas as mobile phase. The temperature was kept at 50 °C for 5 min and programmed to 250 °C for 3 min at rate of 4 °C min^{-1} and programmed to 300 °C at a rate of 25 °C min^{-1}. The injector temperature was set at 250 °C. Slip flow was adjusted at 50 mL min^{-1} and MS was occupied at 70 eV.

2.3 Weight loss, potentiodynamic polarization and EIS measurements

Prior to all measurements, the mild steel samples (0.21% C, 0.38% Si, 0.09% P, 0.01% Al, 0.05% Mn, 0.05% S and 99.21% Fe) were mechanically polished on wet SiC paper successively from 80 to 1500 grade. The specimens were washed thoroughly with double distilled water, defatted by ethanol and finally dried with acetone at hot air before being immersed in the acidic medium.

The corrosive medium of 1 M HCl was prepared by dilution of analytical grade 37% HCl with double distilled water. The test solutions were freshly prepared before each experiment by adding MPEO, at different concentrations, directly into1 M HCl solution.

Weight loss tests have been done out in double-walled glass cell coupled with a thermostat-cooling condenser. The solution capacity was 50 mL. The apparent surface part of mild steel samples used was of circa 6 cm^2. The immersion time for the weight loss tests was 6 hours at room temperature of 308 K in air without bubbling. After the corrosion test, the samples were carefully washed in bi-distilled water, dried and then weighted.

The electrochemical study was performed with a Bio-Logic-Science Instruments® potentiostat piloted with Ec-Lab® software. This potentiostat was coupled to a three-electrode cell with a thermostatted double wall. The mild steel used for the working electrode was identical to the one employed for weight loss tests. The surface area in contact of mild steel was of 1 cm^2. A platinum electrode and a sutured calomel electrode (SCE) were used as auxiliary and reference electrodes, respectively.

Potentiodynamic polarization curves were plotted from -900 to -100 mV at 308 K at a polarization scan rate of 1 mVs^{-1}. Before all experiments, the potential was stabilized at the open circuit potential during a hold time immersion of 30 min.

The electrochemical impedance spectroscopy (EIS) measurements were realized using a transfer function analyser, with a small amplitude a.c. signal (10 mV rms) over a frequency region from 100 kHz to 10 mHz at 308 K with 10 points per decade. Computer program automatically controlled the measurements realized at rest potentials after 30 min of immersion at the corrosion potential, E_{corr}. The EIS spectra were given both in the Nyquist and Bode representations. The impedance data were analysed and fitted, in terms of a suitable electrical circuit, with the simulation Ec-Lab (Bio-Logic) software.

2.4 Surface analysis

The surface morphology of the samples, exposed to the acid solutions, was followed by a scanning electron microscope (SEM) model FEI Quanta 200 equipped with EDAX probe microanalysis of surface. The SEM analysis was complete after 24 h immersion at 308 K, for representative specimens in uninhibited and inhibited solutions.

3. RESULTS AND DISCUSSION

3.1 Characterization and chemical composition of MPEO

Fig. 1 exemplifies the gas chromatography-mass spectral analysis of the sample which was dissolved in hexane.

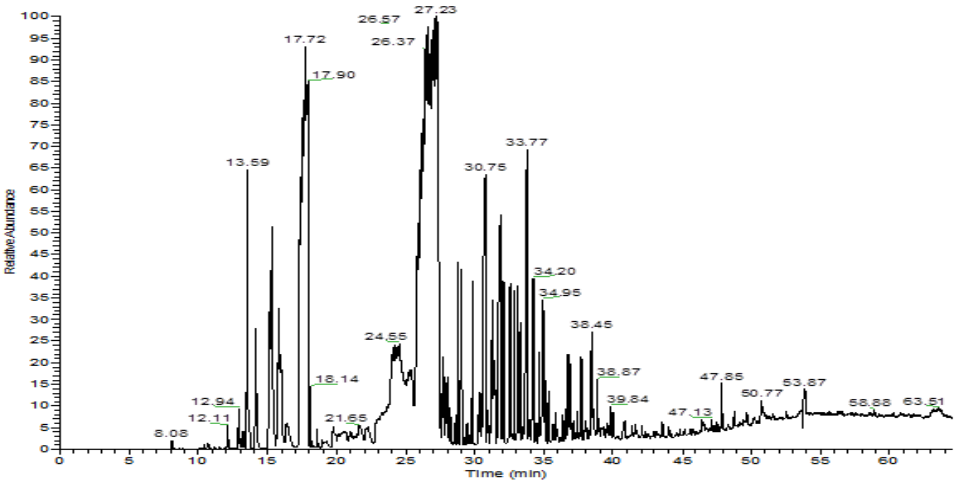

Figure 1. CG-MS MPEO Spectre.

The obtained components were of twenty compounds identified in the MPEO. The obtained constituent percentages of MPEO are summarized in Table 1. The total identified was of 99.55 %.

Table 1. Chemical composition of MPEO.

Constituent	%	Constituent	%
Anthraquinone, 1-(p-fluorophenyl)	42.03	Naphthalene	1.28
Methenolone	26.38	Aristolene	1.17
Selina-3,7(11)-diene	4.75	Menthol	1.12
Longifolene	4.29	Carvyl acetate	1.04
Isoledene	2.96	Carveol acetate	0.98
γ-Terpinene	2.80	δ-Cadinene	0.86
Calamenene	2.17	α-Bulnesene	0.81
Jasmone	2.04	Camphene	0.80
Isocaryophillene	1.72	Cubenol	0.42
Epi-bicyclosesquiphellandrene	1.59	tau.-Muurolol	0.34

MPEO was well dissolved in hydrochloric acid solutions and the chemical structures of the most abundant compounds are given in Fig. 2.

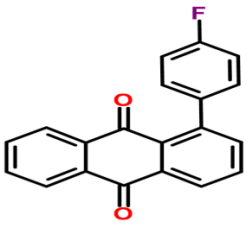

*Anthraquinone, 1-(p-fluorophenyl):$C_{20}H_{11}FO_2$**42.03%***

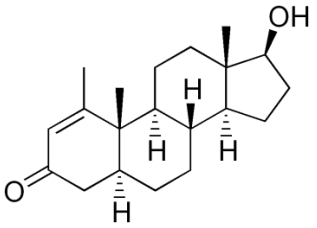

*Methenolone: $C_{20}H_{30}O_2$**26.38%***

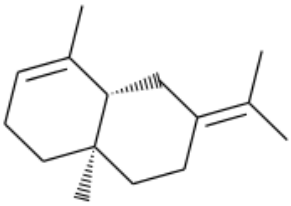

*Selina-3,7(11)-diene:$C_{15}H_{24}$**4.75 %***

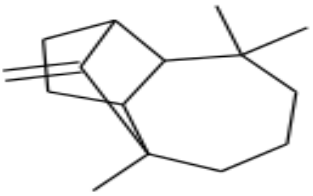

*Longifolene: $C_{15}H_{24}$**4.29%***

Figure 2. Chemical structures of the major components of MPEO.

3.2 Weight loss and SEM studies

The weight loss method is known to be the most widely applied technique for monitoring inhibition efficiency. The corrosion rate in the absence and presence of MPEO is determined via the following Equation 1:

$$W_{corr} = \frac{\Delta m}{S \times t} \quad (1)$$

where Δm *is* the average weight loss of the mild steel specimens, *S* is the total area of the mild steel specimen and *t* is the immersion time. The percentage inhibition efficiency ($\eta_{WL}\%$) is calculated using Equation 2:

$$\eta_{WL}\% = \left(\frac{W_0 - W_{inh}}{W_0} \right) \times 100 \quad (2)$$

where W_0 and W_{inh} are the weight loss values in the absence and presence of MPEO.

Fig. 3 shows both the evolution of weight loss and the corresponding inhibiting efficiency against MPEO concentration. It is evident that there is a tremendous decrease in the mild steel corrosion rate with the addition of MPEO and hence the corrosion rate is concentration dependent. In turn, the inhibiting efficiencies increases with rising inhibitor concentration to reach a maximum value of 86.41 % at 0.7 g L^{-1} of MPEO. Further increase in MPEO concentration does not cause any significant change in the performance of MPEO.

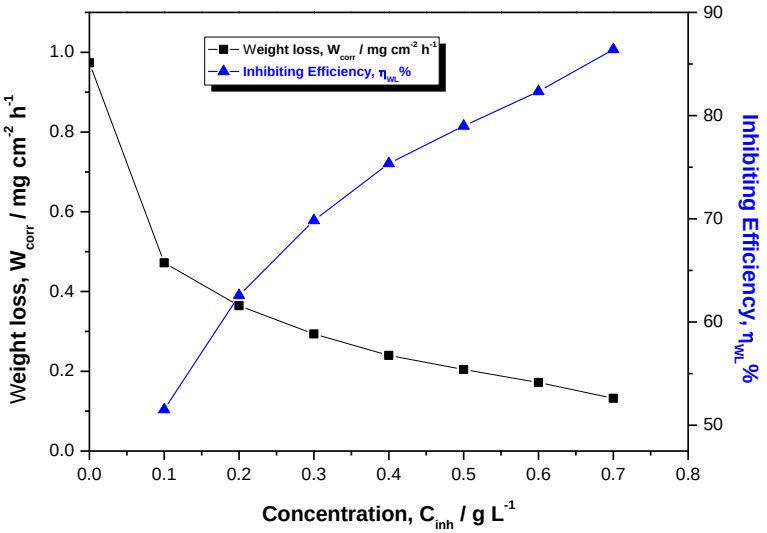

Figure 3. Corrosion rate and inhibiting efficiency of mild steel exposed for 6 h in 1M HCl at different concentrations of MPEO at 308 K.

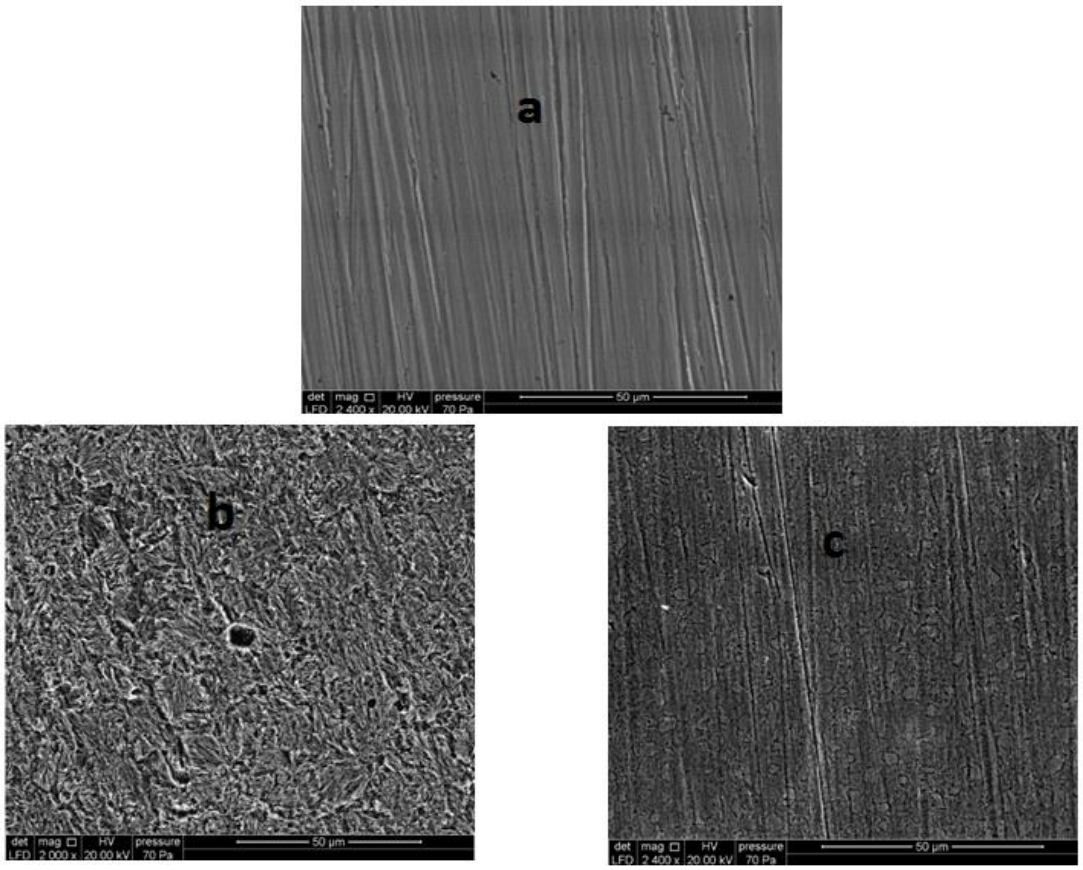

Figure 4. SEM micrographs of the mild steel surface: (a) Metallic surface after being polished, (b) Metallic surface after 24h immersion in 1 M HCl and (c) Metallic surface after 24 h immersion in 1 M HCl with 0.7 g L^{-1} of MPEO

These results indicate that MPEO seems to be a good corrosion inhibitor for mild steel in molar hydrochloric acid medium. The corrosion inhibition property of MPEO is probably due to the inhibitive action of some MPEO components having the ability to be adsorbed onto the mild steel surface and can be considered as effective inhibitors. Indeed, the fact that the major components of MPEO contain lone pairs from heteroatom ketones, Fluor and π-orbitals (═), these can block the active sites and therefore reducing the corrosion rate. Besides, the inhibitive nature of MPEO may also be imputed to a synergistic intermolecular effect of different active constituents present in this essential oil although minor compounds (Table 1).

The scanning electron microscopy (SEM) micrographs (Fig.4a-c) of the surfaces of mild steel strips were recorded. Fig.4a exemplifies the polished steel surface before exposure to the corrosive solution and clearly visible parallel features appear linked to abrading scratches. Fig.4b-c show the SEM micrographs of mild steel surface before and after immersion in molar hydrochloric acid, during 24 hours, with and without MPEO inhibitor in order to see the changes that can occur during the corrosion process. The result of the high-resolution SEM micrograph (50 µm) shows that the metal surface is strongly damaged in the absence of MPEO due to a rapid corrosion attack (Fig. 4b). However, a relatively smoother and less corroded morphology of mild steel surface can be observed with 0.7 g L^{-1} of MPEO (Fig. 4c) for which the best inhibiting efficiency is registered. Consequently, MPEO inhibits the mild steel corrosion in 1 M HCl.

3.3 Potentiodynamic polarization study

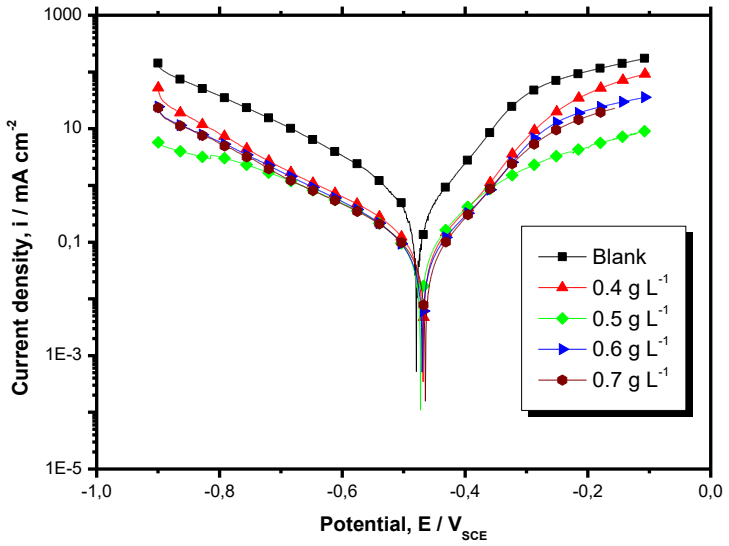

Figure 5. Polarization curves of mild steel in 1 M HCl at different concentrations of MPEO at 308 K.

Most widely corrosion phenomena are of electrochemical type and comprise of reactions on surface corroding metal. Formerly, electrochemical methods can be utilized to evaluate corrosion rates and to characterize corrosion mechanisms. The effect of MPEO concentration on the potentiodynamic anodic and cathodic polarization curves of mild steel is then also studied in 1 M HCl solution.

Fig. 5 illustrates the potentiodynamic polarization curves for mild steel, in acidic solution, in the absence and presence of restricted and representative concentrations of MPEO. The anodic and cathodic

current densities of mild steel in the presence of MPEO have been significantly reduced with respect to that of blank. This decrease is slightly marked with rise of MPEO concentration. Furthermore, a small change in the corrosion potential is registered towards more positive potentials when MPEO is added in 1 M HCl solution.

The anodic branches show a decrease in current densities when compared to the uninhibited acidic solution. This reduction is almost identical for all explored concentrations of MPEO since the corrosion potential until -0.35 V_{SCE}. However, beyond this potential, curves stand out from each other. It is likewise important that the anodic Tafel slopes can easily be identified from these curves as opposed to several published studies which report the appearance of a potential said desorption potential or potential of molecules rearrangement forming an inhibitor film [2,3,12,22].

The cathodic part represent rise to parallel Tafel lines suggesting that the hydrogen evolution is activation controlled. Thus, hydrogen discharge, at the mild steel interface, takes place mainly through a charge transfer mechanism [23,24]. Accordingly, the inhibition process perhaps caused by a simple blocking surface effect, namely the reduction of reaction area on the corroding surface [25]. Thereby, a higher coverage of the essential oil film on the electrode surface can be expected and more pronounced at higher inhibitor concentrations [26].

Consequences of the Tafel fit are ascertained whenever a marker is moved. The default positions of the markers are ± 85 mV and ± 200 mV around E_{corr}; i.e., the explored potential domain, to deduct the electrochemical parameters, is situated beyond ± 85 mV when compared to E_{corr} and in a potential window of ± 115 mV conditioned by a good linearity of the corresponding curves. The software deduces the open circuit potentials, E_{corr} from the linear regressions intersection, the corrosion current density values, i_{corr} and the Tafel slopes, β_c and β_a.The inhibiting efficiency is calculated by using corrosion current densities as given in Equation 3:

$$\eta_{Tafel}\,\% = \left(\frac{i_{corr} - i_{corr/inh}}{i_{corr}} \right) \times 100 \qquad (3)$$

where $i_{corr/inh}$ and i_{corr} are the corrosion current density values with and without inhibitor, respectively, determined by extrapolation of cathodic and anodic Tafel lines to the corrosion potentials using software (Ec-Lab, Bio-Logic).

The examination of the electrochemical parameters given in Table 2 reveals that the corrosion current densities i_{corr} decreases considerably with rise of MPEO concentration. Correspondingly, the inhibition efficiency η_{Tafel} % increases to reach its maximum value of 85 % at 0.7 g L^{-1} of MPEO. This behavior suggests that the MPEO adsorption protective film formed onto the mild steel surface tends to be more and more complete and stable with increasing of MPEO concentration. The presence of MPEO causes a slight shift of corrosion potential when compared to that in the absence of inhibitor. In our study, E_{corr} of mild steel shifts anodically in the range of 7-15 mV compared to the uninhibited solution. From reports in the literature, it has been revealed that if the displacement of E_{corr} is more than 85 mV the inhibitor can be considered as a cathodic or anodic type inhibitor whereas when the displacement of E_{corr} is less than 85 mV, the inhibitor can be considered as mixed type [27]. Consequently, the obtained results indicate that MPEO acts as mixed-type inhibitor.

Table 2. Electrochemical data evaluated from Tafel and Stern & Geary methods for mild steel in 1 M HCl without and with MPEO at 308 K.

	Tafel data					*LPR data*	
C_{inh}	$-E_{corr}$	i_{corr}	$-\beta_c$	β_a	η_{Tafel}	R_p	$\eta_{S\&G}$
$g\ L^{-1}$	mV_{SCE}	$\mu A\ cm^2$	$mV\ dec^{-1}$	$mV\ dec^{-1}$	%	Ωcm^2	%
Blank	479	623	168	176	-	59.4	-
0.4	468	128	192	156	79.33	284	79.08
0.5	472	105	200	119	83.09	309	80.77
0.6	469	97	182	146	84.33	362	83.59
0.7	464	91	192	132	85.37	382	84.45

Further, the values of the cathodic Tafel slopes β_c, in the presence of the inhibitor, significantly not change with the MPEO addition, which implies that its influence on the cathodic reaction does not modify the mechanism of hydrogen evolution discharge [28]. Nevertheless, the values of the slopes of the anodic Tafel lines, β_a, change significantly with the addition of MPEO suggesting that the inhibitor is first adsorbed onto the electrode surface and hindered by simply blocking the anodic reaction sites, and thereby affect the anodic reaction mechanism [29].

The Linear Polarization Resistance (LPR) extraction, with ± 20mV in the vicinity of E_{corr}, is carried out in order to exclude the influence of the surface changes which may occur during polarization at higher over potentials in the case of potentiodynamic polarization method. The corresponding polarization resistance R_p values of mild steel in 1 M HCl, in the absence and presence of different concentrations of MPEO, are also given in Table 2. R_p is determined from the slope of the potential versus current lines. Stern &Geary (S&G) [30] formulated the following Equation 4 for corrosion current calculation:

$$i_{corr} = \frac{C}{R_p} \tag{4}$$

where the constant C is:

$$C = \frac{\beta_a \times \beta_c}{2.303 \times (\beta_a + \beta_c)} \tag{5}$$

It is remarked that R_p increases with increasing the inhibitor concentration. This, in turn slows down the i_{corr} values. The inhibition efficiency $\eta_{S\&G}$ % is calculated as follows:

$$\eta_{S\&G}\% = \left(\frac{R_{p/inh} - R_p}{R_{p/inh}} \right) \times 100 \tag{6}$$

where R_p and $R_{p/inh}$ are the polarisation resistance values without and with MPEO, respectively.

From Table 2, $\eta_{S\&G}$ % increased with inhibitor concentration reaching a maximum value of 84.45 % at 0.7 g L^{-1} for MPEO. This is in logically good agreement with the values of inhibitor efficiency got from Tafel extrapolation along with those obtained from weight loss measurements.

Meanwhile, as a third method, derived from steady-state polarization curves, it is likewise so interesting to search for corrosion kinetic parameters from a fitting by the Stern equation. To do as

such, the global current density values, i, is considered as the summation of two contributions, cathodic and anodic current density, i_c and i_a respectively. Thus, it can be derived from Equation 7:

$$i = i_a + i_c = i_{corr} \times \left(e^{b_a \times (E - E_{corr})} - e^{b_c \times (E - E_{corr})} \right) \quad (7)$$

where b_c and b_a are the Tafel constants of cathodic and anodic reactions (V^{-1}), respectively. These constants are linked to the Tafel slopes β ($Vdec^{-1}$), in usual logarithmic scale, by the following Equation 8:

$$\beta = \frac{\ln 10}{b} \quad (8)$$

However, for this calculation, the potential window is limited in the vicinity of corrosion potential, E_{corr}±100 mV [31]. A significant systematic divergence is sometimes registered for both cathodic and anodic domains.

Fig. 6 shows the results of regressions calculation for the cathodic and anodic branches for mild steel electrode in 1 M HCl at different concentrations of MPEO. A better trend between the experimental and the calculated polarization data is acquired as is indicated in Fig. 6.

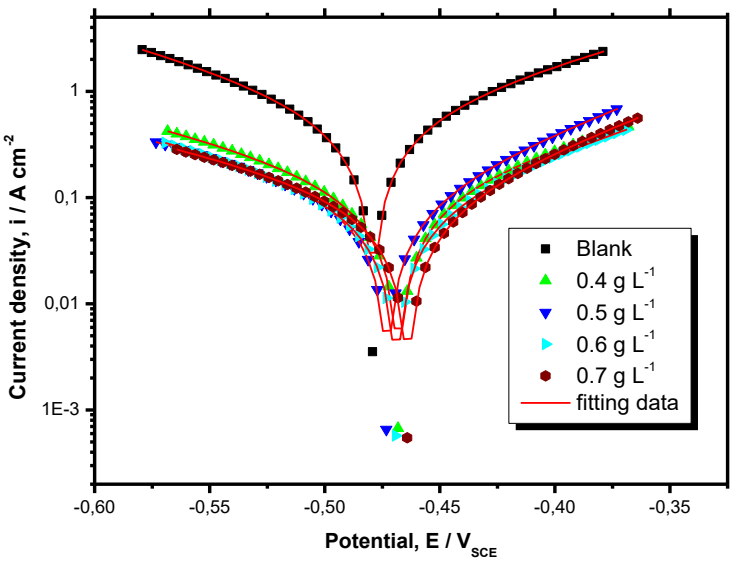

Figure 6. Comparison of experimental (scatter) and fitting (line) data using a nonlinear fitting with Stern Equation for mild steel electrode at different concentrations of MPEO.

To yield quantitative approach, i_{corr}, and E_{corr} are evaluated from the experimental results using a defined function ''Non-linear least squares curve fit'' of graphic software (Origin, Origin-Lab). Hence, the electrochemical parameters, obtained from the Stern extrapolation method, such as $E_{corr}, i_{corr}, \beta_a, \beta_c$, R^2, and χ^2, are reported in Table 3. The fit accuracy χ^2 equation used in this method is defined as follows in Equation 9 [32]:

$$\chi^2 = \frac{1}{N} \sqrt{\sum_{i=1}^{N} (i_{mes,i} - i_{cal,i})^2} \quad (9)$$

where N is the freedom degrees, i_{mes} designates the measured data whereas i_{cal} corresponds to model data calculated from Stern Equation 7. The corresponding inhibiting efficiency is calculated by using corrosion current densities as formulated in Equation 10:

$$\eta_{Stern}\,\% = \left(\frac{i_{corr} - i_{corr/inh}}{i_{corr}} \right) \times 100 \qquad (10)$$

$\eta_{Stern}\,\%$ seems to be similar to that of $\eta_{Tafel}\,\%$. The difference between them is situated in the potential domains from which the overall electrochemical parameters are extracted.

Table 3. Electrochemical data evaluated from Stern method for mild steel in 1 M HCl solution at different concentrations of MPEO at 308 K.

C_{inh} $g\ L^{-1}$	$-E_{corr}$ mV_{SCE}	i_{corr} $\mu A\ cm^{2}$	$-\beta_c$ $mV\ dec^{-1}$	β_a $mV\ dec^{-1}$	R^2	$10^3 \chi^2$	η_{Stern} %
Blank	479±0.52	640±2.4	163±11	167±12	0.999	0.61	-
0.4	468±0.18	138±9.0	192±6	177±5	0.999	0.52	78.45
0.5	472±0.18	102±3.3	196±5	120±4	0.999	0.85	83.97
0.6	469±0.27	92±5.6	175±7	139±6	0.999	0.43	85.48
0.7	464±0.23	88±2.7	189±6	121±5	0.999	0.18	86.22

The statistic chi square value χ^2 relates a measurement of how expectations compare to experimental values. It is observed that a good accuracy of the fitting is obtained, as evidence by an order of 10^{-3} for all the experimental data. On the other hand, the determination coefficient R^2 is a statistical measure of how close the experimental data are when compared to the fitted regression line. It is also known that R^2, or the factor of multiple determinations for multiple regressions, is always between 0 and 1. In general, the elevated the value of R^2, the better model fits the experimental data. From Table 3, an excellent fit is observed with R^2 up to 0.999, which indicates that the experimental results are well described by the Stern model.

Fig. 6 clearly shows that the addition of MPEO in 1 M HCl solution reduces both the anodic mild steel dissolution and the cathodic hydrogen evolution reactions. The reduction described by the Stern method is in agreement with that of the Tafel method (Fig. 5). In reality, the fact that the corrosion potentials are very neighbour justifies the validity of the branches comparison. Moreover, the overall electrochemical parameters, summarized in Table 3, and derived from the Stern method, at all MPEO concentrations, are in very good agreement with those obtained from Tafel method. Thus, the inhibiting efficiencies follow the same trend with a maximum value of 86 % at 0.7 g L^{-1} of MPEO.

3.4 EIS measurements

A better comprehension of the mechanism taking place at the mild steel interface is often attained through impedance measurements. EIS is performed under potentiostatic conditions at E_{corr} and 308 K in the blank and inhibited solution containing different concentrations of MPEO. Before each measurement, the

electrode is left at the open circuit conditions during half an hour as observed for the steady-state experiments. The electrode system does not evolve significantly during EIS measurements.

Nyquist (Z', -Z") and Bode log (f)-log (|Z|) and log (f)–Phase diagrams of the mild steel electrode obtained in 1 M HCl solution in the absence and presence of various concentrations of MPEO, are shown in Fig.7 a-c. The insert diagram in Fig.7a is the one of the uninhibited medium.

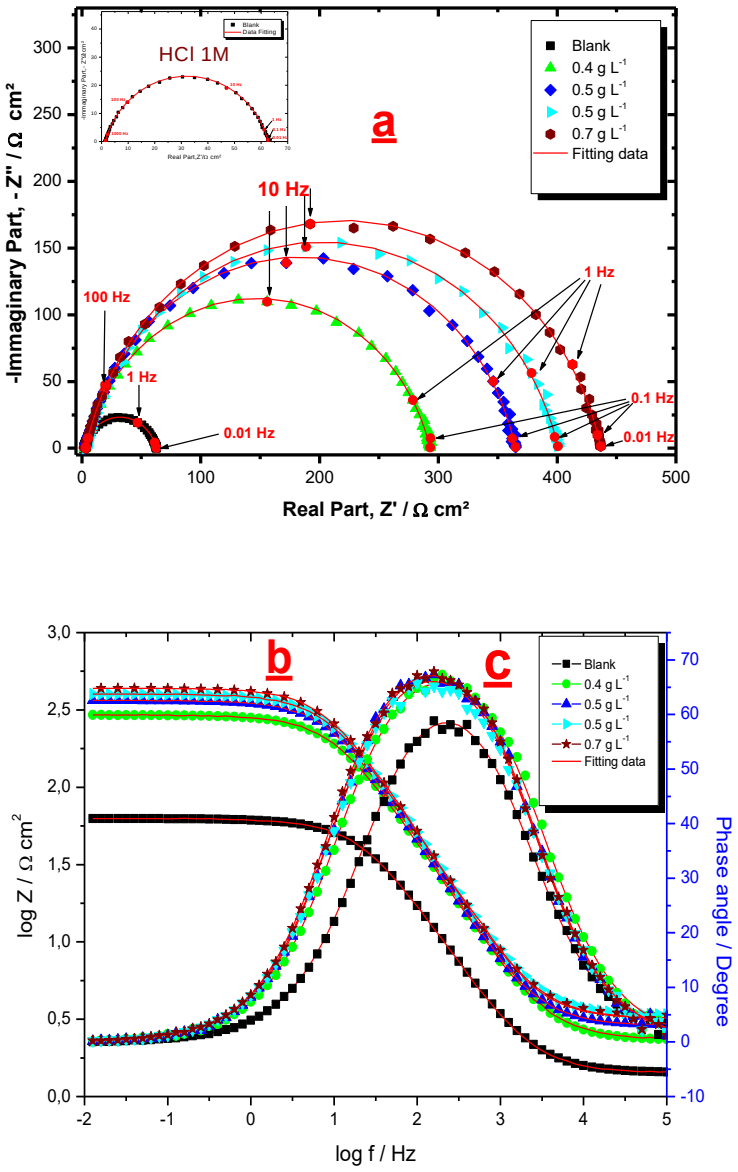

Figure 7. Z', -Z" (**a**) log(f), log (|Z|) (**b**) and log (f), Phase (**c**) diagrams of mild steel in 1M HCl at different concentrations of MPEO at 308 K. The insert is the one in uninhibited medium.

A depressed semicircle, in the Nyquist representation, is registered, and only one-time constant appears in log (f)–log (|Z|) plot, as often obtained in acidic media [33–35]. The presence of MPEO, in 1 M HCl, does not affect the appearance of both the Nyquist and the Bode plots, which suggests a similar corrosion mechanism in the presence of MPEO. The difference from theoretical results is generally attributed

to Cole-Cole [36,37] and/or Cole-Davidson [38] representations inherent to frequency dispersion and commonly attributed to the generation of microscopic roughness at the electrode surface during the corrosion process [39,40]. The existence of single semicircle relates the presence of single charge-transfer process, which is unaffected by the presence of MPEO.

The various impedance results such as R_s, R_t, C_{dl}, τ, n, A and χ'^2 are depicted in Table 4. The χ'^2 given in Equation 11 used in this method, is defined as follows [32]:

$$\chi'^2 = \sum_{i=1}^{n} \frac{\left|Z_{meas}(i) - Z_{model}(f_i, param)\right|^2}{D_i^2} \quad (11)$$

where $Z_{meas}(i)$ is the measured impedance at the f_i frequency, $Z_{model}(f_i, param)$ is function of the chosen model and *param* is the model parameter (R_s, R_t, A). D_i is the normal deviation. Estimates of the margins of error calculated for some parameters are also reported in Table 4. The electrolyte resistance R_s determined between working and reference electrodes can be obtained from the abscissa axis intercept of the semicircle at $f \to \infty$, $R_s \approx 3\ \Omega\ cm^2$ in all studied solutions. Whereas, the charge transfer resistance R_t is calculated from the subtraction in impedance at lower and higher frequencies, i.e. the diameter of the semicircle and the double layer capacitance C_{dl} is determined by a transfer function with the constant phase element *CPE*. Indeed, *CPE* is used to substitute the double layer capacitance for a more accurate fit and is calculated as follows, Equation 12:

$$Z_{CPE} = A^{-1}(j \times \omega)^{-n} \quad (12)$$

In the same Table 4 are shown also the calculated C_{dl}, using the Hsu and Mansfield formula (Equation 13) reported by Hamdani . [41]:

$$C_{dl} = \left(A \times R_t^{1-n}\right)^{\frac{1}{n}} \quad (13)$$

where A is a proportional factor ($\mu F\ s^{n-1}$), j is an imaginary number with j^2 = -1, n is an exponent related to the phase shift which can be used as a measure of surface irregularity and ω is the angular frequency in rad s^{-1}. $\omega_{max} = 2 \times \pi \times f_{max}$, where f_{max} is the frequency at which the imaginary component of the impedance is maximal ($-Z''_{max}$). In first approximation, C_{dl} and the frequency f_{max} are found as represented in Equation14:

$$f(-Z''_{max}) = \frac{1}{2 \times \pi \times \tau} \quad where \quad \tau = R_t \times C_{dl} \quad (14)$$

The impedance diagrams analysis led to research an equivalent circuit which may translate the metal/solution interface behavior, compatible with the shape of the diagrams. According to a classical method, the impedance spectra of Fig. 7 will be interpreted in terms of a simple modified Randles circuit, with one relaxation time constant τ, as given in Fig.8 with a *CPE* in parallel to R_t, the all are in series with another resistor corresponding to the electrolyte solution resistance R_s.

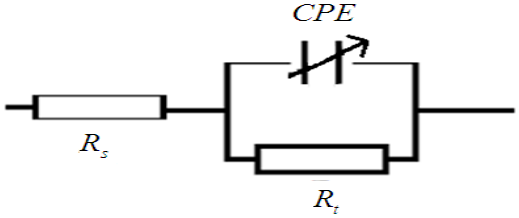

Figure 8. The equivalent circuit used for fitting the impedance spectra.

The quality of fitting to the equivalent circuit is judged by chi square value χ^2 [42]. The corresponding values (0.0376–0.697), reported in Table 4, testify the good quality fitting with the proposed circuit.

It may be assumed, as an approximation, that either $(R_t)^{-1}$ [43] or C_{dl} [44] parameters are directly related to the corrosion rate i_{corr}. The inhibiting efficiency $\eta_{EIS}\%$ got from the charge transfer resistance is calculated as follows, Equation15:

$$\eta_{EIS}\% = \left(\frac{R_{t/inh} - R_t}{R_{t/inh}} \right) \times 100 \quad (15)$$

where R_t and $R_{t/inh}$ are the charge-transfer resistance values without and with inhibitor, respectively.

Table 4. EIS data of mild steel in 1M HCl containing different concentrations of MPEO at 308 K.

C_{inh} $g\ L^{-1}$	R_s $\Omega\ cm^2$	R_t $\Omega\ cm^2$	C_{dl} $\mu F\ cm^{-2}$	τ ms	A $\mu F\ s^{n-1}$	n	φ	χ'^2	η_{EIS} %
Blank	1±0.22	61±0.36	113	6	268±22.10^{-3}	0.826	-0.62	0.0376	-
0.4	2±0.21	290±0.37	50	14	100±1.10^{-3}	0.838	-0.72	0.0697	78.91
0.5	2±0.20	362±0.37	48	17	87±1.10^{-3}	0.852	-0.75	0.0460	82.98
0.6	3±0.20	397±0.37	45	18	86±1.10^{-3}	0.841	-0.74	0.0548	84.59
0.7	3±0.20	433±0.37	44	19	80±1.10^{-3}	0.849	-0.75	0.0493	85.87

The analysis of Table 4 reveals that addition of increasing concentration of MPEO increases R_t and decreases C_{dl}, and consequently enhances $\eta_{EIS}\%$ till reaching its maximum value at 0.7 g L^{-1}. It is to be noted that the diameter of the capacitive loop of the Nyquist plots increases with rise of MPEO concentration without affecting their characteristic features. This behaviour means that the inhibition action of MPEO is related to its adsorption on the metal surface without altering the corrosion mechanism. Furthermore, the magnitude of C_{dl} decreases with increasing MPEO concentrations. This situation can be interpreted as a result of increase in the surface coverage by MPEO, to the soft surface of mild steel or other poorly conductive products such as oxides and hydroxides, which led to an increase in the inhibiting efficiency [45].

The addition of MPEO in 1 M HCl increases slightly the relaxation time constant τ value with an opposite trend of C_{dl} (cf. Table 4). Indeed, in uninhibited and at 0.7 g L^{-1} of MPEO, the interface τ parameter increases from 6 to 19 ms while the C_{dl} value decreases from 113 to 44 µF cm^{-2}, signifying that the charge and discharge rates to the mild steel/solution interface is greatly decreased. This indication shows that there is conformity between the amount of charge that can be stored (i.e., C_{dl}) and the discharge velocity at the interface [29]. It is worth mentioning that the value of the relaxation time constant τ remains almost constant despite the slight increase of circa 4 ms in inhibited media at different concentrations. This finding justifies the choice of the circuit represented in Fig. 8. The thickness of the protective film δ is linked to C_{dl} by the following Equation16:

$$\delta = \frac{\varepsilon \times \varepsilon_0}{C_{dl}} \times S \quad (16)$$

where ε, ε_0, and S stand for the vacuum dielectric constant (ε_0 = *8.854 10^{-14} F cm^{-2}*), the relative dielectric constant, and the surface area, respectively. The decrease in C_{dl}, which can result from an increase in the thickness of the electrical double layer and/or a decrease in local dielectric constant, suggests that MPEO functions by adsorption on the mild steel at the metal/solution interface.

The slopes φ of the plots log(|Z|)-log(f) (Fig. 7b), which correspond to the medium-frequency part, are calculated and the obtained data are also reported in Table 4. In theory, the value of φ should be equal to -1 for an ideal capacitor. However, the experimental φ values range from -0.62 to -0.75, which might be explained by the non-ideal structure of the metal/solution interface [5].

The n value seems to be related with the non-uniform distribution of current as a result of roughness and possible oxide surface defects. When n = 1, *CPE* represents a perfect capacitor. A true capacitive behavior is rarely obtained that is why *CPE* is usually used for data fitting instead of a perfect capacitor. The present study shows that n < 1, in both uninhibited and inhibited media, confirming the surface heterogeneity despite the adsorption of MPEO on the most active adsorption sites of the mild steel surface. As reported in the literature, the slight decrease of n is an indicator of the surface inhomogeneity as a result of the inhibitor's adsorption [41]. An opposite trend is registered in our case which suggests an enhance of homogeneity when MPEO is adsorbed.

3.5 Comparison of the overall results

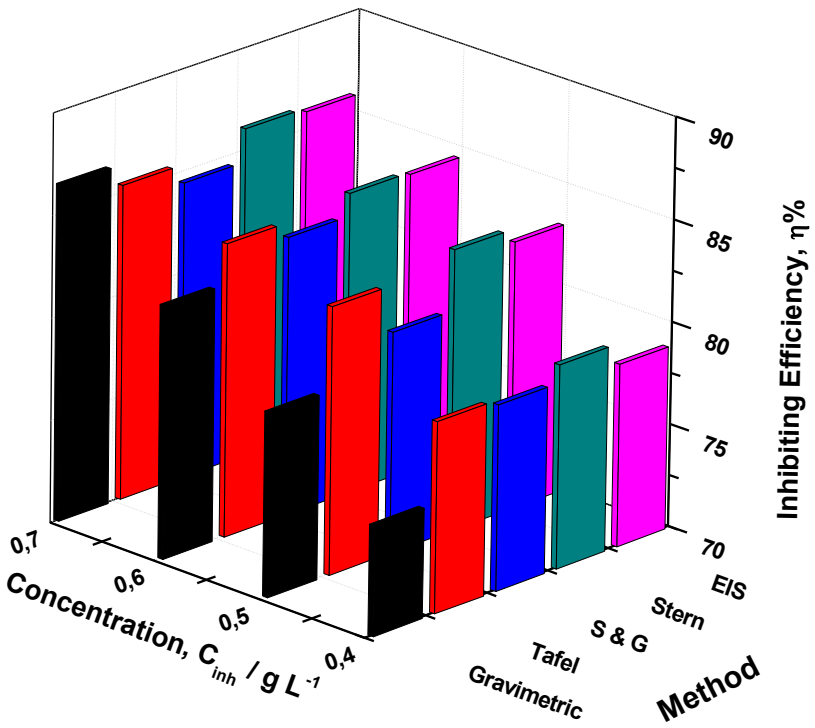

Figure 9. Comparison of the inhibition efficiency η % values obtained by weight loss, potentiodynamic polarisation (Tafel, Stern & Geary and Stern) and EIS methods.

A comparison may be made between inhibition efficiency η % values acquired from the different undertaken weight loss, potentiodynamic polarisation curves (Tafel, Stern &Geary, Stern) and EIS techniques. Fig. 9 shows a histogram of all results which can identify the gaps when comparing the obtained η % values. One can see that whatever the method used, no significant changes are observed in η % values and the same trend is conserved with rise of MPEO concentration when the best inhibiting efficiency always stand for 0.7 g L^{-1} of MPEO. The coincidence between Tafel, Stern & Geary, and Stern methods can suggest that no significant surface changes occur during the polarization measurements at ± 200 mV versus E_{corr}. The values of η % obtained by means of the polarization and EIS experiments are somewhat higher than in the weight loss study but the trends persist the same. These distinctions are most likely due to a more prominent to the variant contact time in the corrosive solution which are 6 h and 1 h for weight loss and electrochemical techniques, respectively. It would then be able to be inferred that there is a best correlation with the five methods apply in this examination at all studded concentrations and that MPEO is an effective corrosion inhibitor for mild steel in 1 M HCl.

3.6 Effect of temperature

It is worthwhile considered to investigate the temperature effect as it can modify the interaction among the metal electrode and the acidic medium in the presence and absence of MPEO. Table 5 illustrates the impact of temperature on metallic dissolution using weight loss measurements in the temperature range from 308 to 348 K.

It is observed that the weight loss is circa 13 and 15 times greater, at 348 K when compared to 308 K, in uninhibited and inhibited media, respectively. However, it is worth to recall that the presence of MPEO slows down the average corrosion rate, at all the studied temperatures, by 7 times by comparison to the free medium. In contrast, the inhibitive efficiency seems to be little sensitive to the effect of temperature.

Table 5. Weight loss results of the mild steel corrosion with and without addition of 0.7 g L^{-1} of MPEO studied at different temperatures and after 2 h of immersion period.

Temperature	Corrosion rate W_{corr}		η_{WL}
K	*mg cm^{-2} h^{-1}*		*%*
	Blank	MPEO	
308	0.9736	0.1323	86.41
318	2.1325	0.2944	86.19
328	4.3174	0.6410	85.15
338	8.3047	1.2399	85.06
348	12.8556	1.9809	84.59

The activation energies of mild steel dissolution process in free and inhibited media are calculated using Arrhenius Equation 17:

$$W_{corr} = F\, e^{\frac{-E_a}{RT}} \quad (17)$$

where F is a frequency factor, E_a is the apparent activation corrosion energy, R is the gas constant and T the absolute temperature. Plotting $\ln W_{corr}$ versus $1/T$ gives straight lines as revealed from Fig. 10.

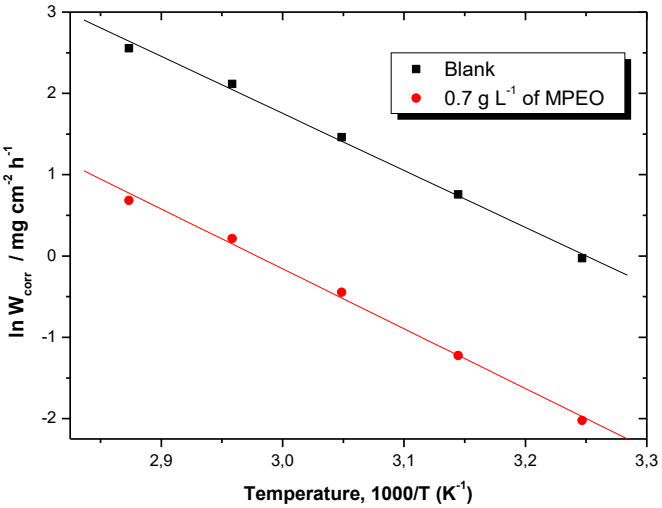

Figure 10. Arrhenius plots of mild steel in 1 M HCl with and without 0.7 g L^{-1} of MPEO.

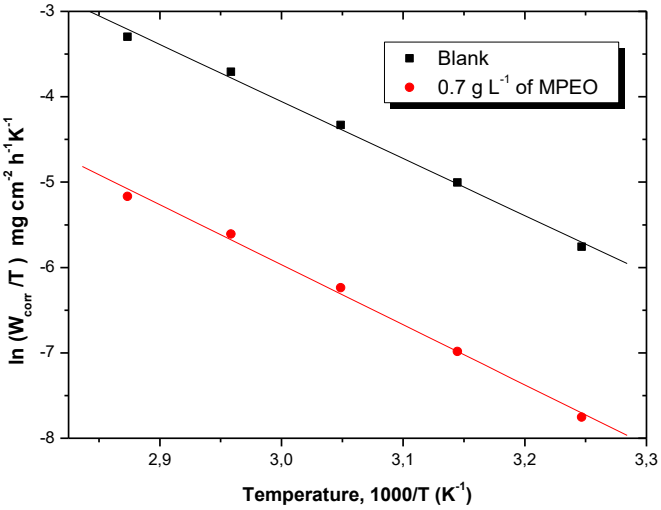

Figure 11. Variation of $\ln(W_{corr}/T)$ vs. $1/T$ in 1 M HCl with and without 0.7 g L^{-1} of MPEO.

The kinetic parameters are evaluated from the effect of temperature by using an alternative formulation of Arrhenius relationship also called transition Equation 18 [46]:

$$W_{corr} = \frac{RT}{N\,h} e^{\frac{\Delta S^*}{R}}\, e^{\frac{-\Delta H^*}{RT}} \quad (18)$$

where N is the Avogadro's number, h is the Plank's constant. ΔS^* and ΔH^* the entropy and enthalpy of activation, respectively.

Figure 11 shows the plots of $\ln(W_{corr}/T)$ against $1/T$ for MPEO and straight lines are obtained with a slope of $(-\Delta H^*/R)$ and an intercept of $\ln(R/Nh)+\Delta S^*/R$ from which the values of ΔH^* and ΔS^* are calculated, respectively.

Table 6 collects the values of activation parameters (E_a, ΔH^* and ΔS^*) for mild steel dissolution in the corrosive media with and without addition of 0.7 g L^{-1} of MPEO. In general, if an inhibitor causes a rise in E_a value when compared to the uninhibited solution, this could be frequently explicated as a suggestion for the formation of an adsorptive film by physisorption mechanism [47,48]. While, a decrease in E_a value when compared to the uninhibited solution is often interpreted as an indication of chemisorption [49]. Furthermore, Popova [50] has also discussed the evolution not only of E_a but also those of pre-exponential factor and inhibiting efficiency to get information on the adsorption mode. In fact, physisorption is accepted, although the inhibiting efficiency decreases with rise of temperature and the E_a is higher than that in inhibitor's free as well the pre-exponential factor which becomes greater in the presence of inhibitor.

Table 6. The values of activation parameters F, E_a, ΔH^*, ΔS^* for mild steel in 1M HCl in the absence and presence of 0.7 g L^{-1} of MPEO.

Kinetic parameter	Blank	MPEO
F / mg cm^{-2} h^{-1}	7.8089× 10^9	3.3416× 10^9
E_a / kJ mol^{-1}	58	61
ΔH^* / kJ mol^{-1}	55	58
ΔS^* / J K^{-1} mol^{-1}	-64	-71
E_a - ΔH^* / kJ mol^{-1}	3	3

In the present study, the obtained apparent activation energy values are 58 and 61 kJ mol^{-1} for blank, and at 0.7 g L^{-1} of MPEO, respectively. This indicates that the presence of MPEO inhibitor in aggressive solution apparently does not considerably affect the E_a value of the metal dissolution. Comparable results have been described by Hammouti when using *Lavender oil*, and *Pennyroyal mint* oil in acidic solutions [20,51]. The frequency factor F decreases by circa two times while η_{WL}% decreases very slightly and remains higher close to 86 % though temperature rising which go together with a slow increase of E_a by 3 kJ mol^{-1}. These finding testify that physisorption constitutes the most probable type of adsorption of MPEO onto mild steel surface. This electrostatic or physical adsorption can be understood because of the acidic medium nature in which by protonation of the MPEO components (having heteroatom), the molecules become positively charged and can interact with previously adsorbed chloride anions Cl^- at the positively charged surface [41].

Besides, Table 6 reveals that the positive value of activated enthalpy ΔH^* means that the process is an endothermic process and it needs more energy to achieve the activated state or equilibrium state [52,53]. It is to be noted that E_a and ΔH^* values vary similarly allowing to confirm the well-known thermodynamic Equation 19 between E_a and ΔH^* as exposed in Table 6 [54]:

$$\Delta H^* = E_a - (R \times T) \quad (19)$$

Concerning the entropy of activation ΔS^*, it is clear that the entropy ΔS^* increases negatively in the presence of MPEO than that in the blank one. This reflects the formation of an ordered stable layer of MPEO onto the mild steel surface electrode [55]. The decrease of ΔS^* in inhibited medium implies that the activation of MPEO in the rate-determining step represents dissociation rather than an association step, meaning a decrease in disordering taking place on moving from reactants to activated complex [56]. This finding is in agreement with those of other co-workers [57,58].

3.7. Adsorption isotherm

The adsorption isotherm provides insights into the mechanism of corrosion inhibition. So, the determination of relation among corrosion inhibition and adsorption is of great importance. The adsorption of inhibitor molecules at the electrode/solution interface takes place through the substitution of water molecules according to Equation 20:

$$Org_{(sol)} + xH_2O_{(ads)} \leftrightarrow Org_{(ads)} + xH_2O_{(sol)} \quad (20)$$

where $Org_{(sol)}$ and $Org_{(ads)}$ are organic molecules in the solution and adsorbed on mild steel surface, respectively.

Table 7. The different linearized isotherm models undertaken in the present study.

Isotherm	*Linearized form*	*Equation*
Langmuir	$\frac{C_{inh}}{\theta} = \frac{1}{K_{ads}} + C_{inh}$	(22)
El-Awady	$\log\left(\frac{\theta}{1-\theta}\right) = y \log K_{ads} + y \log C_{inh}$	(23)
Flory-Huggins	$\log(\frac{\theta}{C_{inh}}) = \log x K_{ads} + x \log(1-\theta)$	(24)
Langmuir-Freundlich	$\log(C_{inh}) = -\log K_{ads} + \frac{1}{m} \log(\frac{\theta}{1-\theta})$	(25)
Temkin	$\theta = -\frac{1}{2 \times a} \ln K_{ads} - \frac{1}{2 \times a} \ln C_{inh}$	(26)
Dubinin-Radushkevich	$\ln \theta = \ln \theta_{\max} - P \times \sigma^2$	(27)
Freundlich	$\ln \theta = \ln K_{ads} + z \ln C_{inh}$	(28)
Frumkin	$\ln C_{inh}\left(\frac{1-\theta}{\theta}\right) = -\ln K_{ads} - 2d\theta$	(29)

The surface coverage θ values are followed from weight loss, dc polarization methods (Tafel, Stern & Geary, Stern), and EIS measurements at various concentrations of MPEO at 308 K according to Equation 21.

$$\theta = \frac{\eta\%}{100} \quad (21)$$

Several adsorption isotherms are assessed and reported in Table 7. The adsorption models including Langmuir, El-Awady, Flory-Huggins, Freundlich, Dubinin-Radushkevich, Langmuir-Freundlich, Temkin and Frumkin isotherms are applied to fit the surface coverage values at different concentrations of MPEO. On the basis of isotherms criteria [59–61], θ is related to the inhibitor concentration C_{inh} via Equations 22-29 given in Table 7:

where $1/y$ gives the number of H_2O molecules removed by one inhibitor molecule. x is a size parameter and constitute a measure of the number of adsorbed water molecules replaced by a given inhibitor molecule. z is the constant describing the nature of mild steel/medium (MPEO) interface, where $0 \prec z \prec 1$. m is the heterogeneity parameter ($0 < m < 1$) is the heterogeneity parameter which characterizes the distribution of adsorption energy at different sites on a non-ideal surface. $\theta_{\max}$ is the maximum surface coverage and σ is the polany potential and can be estimated from the following Equation 30:

$$\sigma = RT(1 + \frac{1}{C_{inh}}) \quad (30)$$

The constant $\theta_{\max}$ and P (mol^2 kJ^{-2}) are estimated from the intercept and slope of the plot, respectively. And E, which is the transfer energy of one mole of adsorbate from infinity (bulk solution) to the surface of the adsorbent given by Equation 31:

$$E = \frac{1}{\sqrt{2P}} \quad (31)$$

a and d represent interactions factors among adsorbed molecules (these interaction parameters may be negative or positive: $a \text{ or } d \prec 0$ indicates repulsion force, $a \text{ or } d \succ 0$ shows the lateral attraction between adsorbed organic molecules. K_{ads}, expressed in L g^{-1}, is the adsorption coefficient or adsorption equilibrium constant which is related to the standard Gibbs free energy of adsorption, $\Delta_r G^0_{ads}$, in kJ mol^{-1}, according to Equation 32 [62]:

$$K_{ads} = \frac{1}{C_{H_2O}} e^{\frac{-\Delta_r G^0_{ads}}{RT}} \quad (32)$$

where R is the universal gas constant, T the thermodynamic temperature and the concentration of water in the solution is 1000 g L^{-1}.

The straight lines are traced using the least squares method. The experimental data (points) and fitting data (lines) for the best isotherm model are plotted in Figure 12.

To select the isotherm that good fit to experimental results, R^2 was utilized. The best fitting was calculated with the value of R^2 reaches to 0.999 and the fitted line gives a slope very close to unity, which suggests that the experimental results can obtain by Langmuir isotherm. This isotherm postulates that the energy of adsorption is independent of θ and it is no interaction among the adsorbed compounds contained in MPEO. Moreover, Langmuir isotherm accepts that the mild steel surface contains a fixed number of adsorption sites, and each holds one adsorbed species [21].

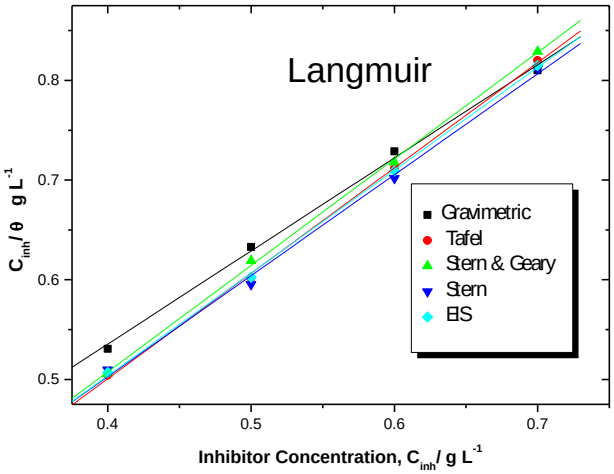

Figure 12. Langmuir isotherm model of MPEO onto the mild steel obtained from five undertaken methods.

Table 8. Parameters values issued from linearized Langmuir adsorption isotherm model for the adsorption of MPEO onto the mild steel surface in 1 M HCl at 308 K.

Isotherm	Method	R^2	*Slope*	K_{ads}	$\Delta_r G^0_{ads}$
	Weight loss	0.997	0.933	6	-22
	Tafel	0.999	1.056	12	-24
	S&G	0.999	1.067	12	-24
	Stern	0.996	1.012	10	-23
	EIS	0.999	1.031	10	-23

Finally, $\Delta_r G^0_{ads}$ is calculated from Equation 32 despite the controversies met in the literature [20,63] because the component(s) of the essential oil components remain(s) unknown. In contrary, other researchers [17–19] calculate this variable and discussed it on the basis of $\Delta_r G^0_{ads}$ values around –20 kJ mol^{-1} or less negative are related to an electrostatic interaction between charged mild steel surface and charged essential oil molecules; that is physisorption. whereas, those of –40 kJ mol^{-1} or more negative apply charge sharing or transfer from MPEO molecules to the electrode surface to form a coordinate type bond; i.e., chemisorption [64]. Thus, it remains not easy to discriminate either chemisorption or physisorption simply based on these criteria, particularly when charged species are adsorbed. The opportunity of Coulomb interactions between adsorbed anions and specifically adsorbed cations can increase the Gibbs energy even if no chemical bond appears [66]. Once again, referring to the whole results and on the basis of the obtained $\Delta_r G^0_{ads}$, it seems difficult to be able to pronounce in a categorical way on both mechanisms.

4. CONCLUSION

The corrosion inhibition of mild steel in molar hydrochloric medium by *Mentha Piperita* essential oil (MPEO) was studied using common weight loss, electrochemical and SEM techniques. According to experimental results, it could be concluded that:

1. MPEO constitutes an effective corrosion inhibitor for the mild steel in 1 M HCl. The inhibiting efficiency is concentration dependent reaching value up to 87% at 0.7 g L^{-1}.
2. The high-resolution scanning electron microscopy micrograph indicates that the surface morphology shown in the presence of MPEO is significantly different and more regular than that obtained in free inhibitor medium.
3. The potentiodynamic polarization curves are three times explored with Tafel, Stern & Geary, Stern methods and show that MPEO acts as mixed type inhibitor. No significant surface change can be registered in the potential window ranged from - 200 mV to + 200 mV vs. the corrosion potential.
4. EIS measurements studies reveal that the MPEO reduced the corrosion rate by increasing the resistance of the system, and all the diagrams are interpreted in terms of an appropriate equivalent circuit.
5. The overall results derived from weight loss, (Tafel, Stern & Geary, Stern) polarizations, and EIS measurements are in fairly good agreement.
6. The adsorption of MPEO molecules obeys to Langmuir adsorption isotherm model.

References

1. R. Baboian, Corrosion Tests and Standards: Application and Interpretation Second Edition, 2009.
2. R. Solmaz, *Corros. Sci.*, 52 (2010) 3321.
3. B. Zerga, B. Hammouti, M. Ebn Touhami, R. Touir, M. Taleb, M. Sfaira, M. Bennajeh, and I. Forssal, *Int. J. Electrochem. Sci.*, 7 (2012) 471.
4. K. Benbouya, B. Zerga, M. Sfaira, M. Taleb, M.E. Touhami, and B. Hammouti, *Int. J. Electrochem. Sci.*, 7 (2012) 6313.
5. R. Solmaz, *Corros. Sci.*, 79 (2014) 169.
6. P.B. Raja, and M.G. Sethuraman, *Mater. Lett.*, 62 (2008) 113.
7. Z. Bensouda, E. Elassiri, M. Galai, M. Sfaira, A. Farah, and M.E. Touhami, *J. Mater. Environ. Sci.*, 9 (2018) 1851.
8. J. Bhawsar, P.K. Jain, and P. Jain, *Alexandria Eng. J.*, 54 (2015) 769.
9. M. Ramananda Singh, P. Gupta, and K. Gupta, *Arab. J. Chem.*, (2013) 0.
10. M. Benabdellah, M. Benkaddour, B. Hammouti, M. Bendahhou, and A. Aouniti, *Appl. Surf. Sci.*, 252 (2006) 6212.
11. L. Majidi, Z. Faska, M. Znini, S. Kharchouf, A. Bouyanzer, and B. Hammouti, *J. Mater. Environ. Sci.*219 (2010) 4 ,.
12. M. Znini, G. Cristofari, L. Majidi, A. Ansari, A. Bouyanzer, J. Paolini, J. Costa, and B. Hammouti, *Int. J. Electrochem. Sci*, 7 (2012) 3959.
13. M. Chraibi, K.F. Benbrahim, H. Elmsellem, A. Farah, I. Abdel-Rahman, B. El Mahi, Y. Filali Baba, K. Kandri Rodi, and F. Hlimi, *J. Mater. Environ. Sci.*, 8 (2017) 972.
14. M. Belkhaouda, L. Bammou, R. Salghi, O. Benali, A. Zarrouk, E.E. Ebenso, and B. Hammouti, *J. Mater. Environ. Sci.*, 4 (2013) 1042.
15. N. Lahhit, a Bouyanzer, J.-M. Desjobert, B. Hammouti, R. Salghi, J. Costa, C. Jama, F. Bentiss,

and L. Majidi, *Port. Electrochim. Acta*, 29 (2011) 127.
16. L. Afia, R. Salghi, E. Bazzi, L. Bazzi, M. Errami, O. Jbara, S.S. Al-Deyab, and B. Hammouti, *Int. J. Electrochem. Sci.*, 6 (2011) 5918.
17. E. Chaieb, A. Bouyanzer, B. Hammouti, and M. Benkaddour, *Appl. Surf. Sci.*, 246 (2005) 199.
18. K. Boumhara, M. Tabyaoui, C. Jama, and F. Bentiss, *J. Ind. Eng. Chem.*, 29 (2015) 146.
19. J. Halambek, K. Berković, and J. Vorkapić-Furač, *Corros. Sci.*, 52 (2010) 3978.
20. B. Zerga, M. Sfaira, Z. Rais, M. Ebn Touhami, M. Taleb, B. Hammouti, B. Imelouane, and A. Elbachiri, *Matériaux Tech.*, 97 (2009) 297.
21. M.H. Hussin, A. Abdul, M. Nasir, M. Ibrahim, and N. Brosse, *Measurement*, 78 (2016) 90.
22. F. Bentiss, M. Outirite, M. Traisnel, H. Vezin, M. Lagrenée, and B. Hammouti, *Int. J. Electrochem. Sci*, 7 (2012) 1699.
23. A.Y. Musa, A.A.H. Kadhum, A.B. Mohamad, and M.S. Takriff, *Corros. Sci.*, 52 (2010) 3331.
24. L. Li, X. Zhang, J. Lei, J. He, S. Zhang, and F. Pan, *Corros. Sci.*, 63 (2012) 82.
25. I. Ahamad, and M.A. Quraishi, *Corros. Sci.*, 51 (2009) 2006.
26. Q.B. Zhang, and Y.X. Hua, *Electrochim. Acta*, 54 (2009) 1881.
27. O.L. Riggs. Jr., Corrosion Inhibitors, 2nd Editio, C. C. Nathan, Houston, 1973.
28. A. Ansari, M. Znini, I. Hamdani, L. Majidi, A. Bouyanzer, and B. Hammouti, *J. Mater. Environ. Sci.*, 5 (2014) 81.
29. M. Tourabi, K. Nohair, M. Traisnel, C. Jama, and F. Bentiss, *Corros. Sci.*, 75 (2013) 123.
30. M. Stern, and A.L. Geary, *J. Electrochem. Soc.*, 104 (1957) 559.
31. A. Rochdi, O. Kassou, N. Dkhireche, R. Touir, M. El Bakri, M. Ebn Touhami, M. Sfaira, B. Mernari, and B. Hammouti, *Corros. Sci.*, 80 (2014) 442.
32. B.P.F. William H. Press, Saul A. Teukolsky, William T. Vetterling, Numerical Recipes in C: The Art of Scientific Computing, 1992.
33. M. Elayyachy, A. El Idrissi, and B. Hammouti, *Corros. Sci.*, 48 (2006) 2470.
34. K. Tebbji, I. Bouabdellah, a. Aouniti, B. Hammouti, H. Oudda, M. Benkaddour, and a. Ramdani, *Mater. Lett.*, 61 (2007) 799.
35. A. Chetouani, M. Daoudi, B. Hammouti, T. Ben Hadda, and M. Benkaddour, *Corros. Sci.*, 48 (2006) 2987.
36. K.S. Cole, and R.H. Cole, *J. Chem. Phys.*, 9 (1941) 341.
37. S. Duval, M. Keddam, M. Sfaira, A. Srhiri, and H. Takenouti, *J. Electrochem. Soc.*, 149 (2002) B520.
38. D.W. Davidson, and R.H. Cole, *J. Chem. Phys.*, 19 (1951) 1484.
39. K.Juttner, *Electrochim. Acta*, 35 (1990) 1501.
40. F. Deflorian, V.B. Miskovic-Stankovic, P.L. Bonora, and L. Fedrizzi, *Corrosion*, 50 (1994) 438.
41. N. El Hamdani, R. Fdil, M. Tourabi, C. Jama, and F. Bentiss, *Appl. Surf. Sci.*, 357 (2015) 1294.
42. P.B. Raja, A.K. Qureshi, A. Abdul Rahim, H. Osman, and K. Awang, *Corros. Sci.*, 69 (2013) 292.
43. J. Mabrour, M. Akssira, M. Azzi, M. Zertoubi, N. Saib, A. Messaoudi, A. Albizane, and S. Tahiri, *Corros. Sci.*, 46 (2004) 1833.
44. M. Lagren, *Corros. Sci.*, 44 (2002) 573.
45. A. Popova, and M. Christov, *Corros. Sci.*, 48 (2006) 3208.
46. B. Zerga, A. Attayibat, M. Sfaira, M. Taleb, B. Hammouti, M. Ebn Touhami, S. Radi, and Z. Rais, *J. Appl. Electrochem.*, 40 (2010) 1575.
47. H. Zarrok, A. Zarrouk, B. Hammouti, R. Salghi, C. Jama, and F. Bentiss, *Corros. Sci.*, 64 (2012) 243.
48. T. Swuer;, and A. Brand;, *Electrochim. Acta*, 26 (1981) 1209.
49. I. Dehri, and M. Özcan, *Mater. Chem. Phys.*, 98 (2006) 316.
50. A. Popova, *Corros. Sci.*, 49 (2007) 2144.
51. A. Bouyanzer, B. Hammouti, and L. Majidi, *Mater. Lett.*, 60 (2006) 2840.
52. N.D. Gowraraju, S. Jagadeesan, K. Ayyasamy, L.O. Olasunkanmi, E.E. Ebenso, and C.

Subramanian, *J. Mol. Liq.*, 232 (2017) 9.
53. A. Popova, E. Sokolova, S. Raicheva, and M. Christov, *Corros. Sci.*, 45 (2003) 33.
54. L. Herrag, B. Hammouti, S. Elkadiri, A. Aouniti, C. Jama, H. Vezin, and F. Bentiss, *Corros. Sci.*, 52 (2010) 3042.
55. A. Yurt, A. Balaban, S.U. Kandemir, G. Bereket, and B. Erk, *Mater. Chem. Phys.*, 85 (2004) 420.
56. A. Hamdy, and N.S. El-Gendy, *Egypt. J. Pet.*, 22 (2013) 17.
57. S. Aloui, I. Forsal, M. Sfaira, M.E. Touhami, M. Taleb, M.F. Baba, and M. Daoudi, *Port. Electrochim. Acta*, 27 (2009) 599.
58. Y. Aouine, M. Sfaira, M. Ebn Touhami, A. Alami, B. Hammouti, M. Elbakri, A. El Hallaoui, and R. Touir, *Int. J. Electrochem. Sci.*, 7 (2012) 5400.
59. I. Langmuir, *Const. Solids Liq.*, 252 (1916) 2221.
60. M. Faustin, A. Maciuk, P. Salvin, C. Roos, and M. Lebrini, *Corros. Sci.*, 92 (2015) 287.
61. A.A. El-Awady, B.A. Abd-El-Nabey, and S.G. Aziz, *J. Electrochem. Soc.*, 139 (1992) 2149.
62. M.S. Morad, *Corros. Sci.*, 50 (2008) 436.
63. A. Khadraoui, A. Khelifa, M. Hadjmeliani, R. Mehdaoui, K. Hachama, A. Tidu, Z. Azari, I.B. Obot, and A. Zarrouk, *J. Mol. Liq.*, 216 (2016) 724.
64. M. Behpour, S.M. Ghoreishi, N. Mohammadi, N. Soltani, and M. Salavati-Niasari, *Corros. Sci.*, 52 (2010) 4046.
65. M. Srivastava, P. Tiwari, S.K. Srivastava, R. Prakash, and G. Ji, *J. Mol. Liq.*, 236 (2017) 184.
66. A.K. Singh, and M.A. Quraishi, *Corros. Sci.*, 53 (2011) 1288.